Supplementary Material for *Descanning: From Scanned to the Original Images with a Color Correction Diffusion Model*

Junghun Cha[1*], Ali Haider[1*], Seoyun Yang[1], Hoeyeong Jin[1], Subin Yang[1], A. F. M. Shahab Uddin[2], Jaehyoung Kim[1], Soo Ye Kim[3], Sung-Ho Bae[1]

[1] Kyung Hee University
[2] Jashore University of Science and Technology
[3] Adobe Research
{jhcha08, alihaider, 2019101234, wlsghldud, ysb8049, crux153, shbae}@khu.ac.kr, s.uddin@just.edu.bd, sooyek@adobe.com

Implementation Details

Denoising Network Architecture

DescanDiffusion employs a denoising network based on the UNet (Ronneberger, Fischer, and Brox 2015) architecture, denoted as ϵ_θ, which is comprised of four downsampling and four upsampling blocks. Each of these blocks consists of two residual (He et al. 2016) blocks, where each block involves 2D convolutions followed by the SiLU (Elfwing, Uchibe, and Doya 2018) activation function. Two-stride 2D convolutions are used for downsampling feature maps, while nearest neighbor upsampling followed by 2D convolution is utilized for upsampling. To encode the time steps t and color correction vector v_c, the Transformer sinusoidal positional encoding (Vaswani et al. 2017) and color projection network are exploited. The resulting embeddings are then summed (Nichol and Dhariwal 2021) and fed into each residual block for time step and color conditioning. The first downsampling block has a filter width of 64, which is doubled after each downsampling block.

Training of DescanDiffusion

Firstly, we pre-train the color encoder based on ResNet-34 (He et al. 2016) for 2.7×10^4 iterations using Adam optimizer (Kingma and Ba 2014), with a batch size of 32 and a learning rate of 3.0×10^{-4}. To train the conditional noise predictor, we follow Algorithm 1 in the main paper. During the training of the Local Generative Refinement Diffusion Model (LGRDM), we fix the total number of diffusion steps to 2000 and set the batch size to 16. We use a fixed learning rate of 1.0×10^{-4} throughout the training process with the Adam optimizer. The denoising network requires approximately 72 hours to train on 8 NVIDIA GeForce RTX 3090 GPUs. Both the color encoder and conditional denoising networks are trained with images from the DESCAN-18K training set that have been resized to a resolution of 512×512. Note that the comparison models mentioned in Table 1 and 2 of the main paper are also trained with resized 512×512 images from the DESCAN-18K training set.

[*]These authors contributed equally.

Copyright © 2024, Association for the Advancement of Artificial Intelligence (www.aaai.org). All rights reserved.

Number of Reverse Steps and Ablation Study for the Ratio of Synthetic Data

Ori. : Syn.	PSNR (dB) ↑	SSIM ↑	LPIPS ↓	FID ↓	T_o
100 : 0	23.40	0.8717	0.042	13.51	200
75 : 25	23.43	0.8736	0.044	14.60	10
50 : 50	23.43	0.8627	0.049	21.59	10
25 : 75	23.52	0.8722	0.047	16.25	10
0 : 100	23.47	0.8690	0.049	18.32	10

Table 1: Ablation study for the ratio of synthetic data. Ori. : Syn. denotes the ratio of original data to synthetic data in the training set. The baseline is a model trained only with original data (100:0). Red and blue fonts represent the 1^{st} and 2^{nd} rank values in the cases of using synthetic data, respectively.

The optimal number of reverse steps T_o needed for DescanDiffusion is determined through empirical testing, where a subset of the validation set is evaluated with varying numbers of reverse steps to observe its performance. To evaluate the effect of reverse steps on performance, 30 images from the validation set are chosen randomly and inferred using Algorithm 2 in the main paper. The number of reverse steps is then adjusted between 10 to 1000. The quality of descanned images is assessed for each set of reverse steps using PSNR, SSIM (Wang et al. 2004), LPIPS (Zhang et al. 2018), and FID (Heusel et al. 2017). The process of selecting T_o is repeated for every synthetic data ratios set ({100:0, 75:25, 50:50, 25:75, 0:100}).

The performance according to the number of steps for different training set ratios is depicted in Fig. 1. The rapid deterioration of performance is evident across all variants of DescanDiffusion when trained on sequences containing synthetic data, whereas the performance of training with the original DESCAN-18K (the purple lines in Fig. 1) remains consistent even after a large number of steps. This is because both the training set and the validation set consist of images scanned by the same types of scanners. Hence, the distribution of training and validation data is mostly similar, leading to a consistent performance by the original data without the

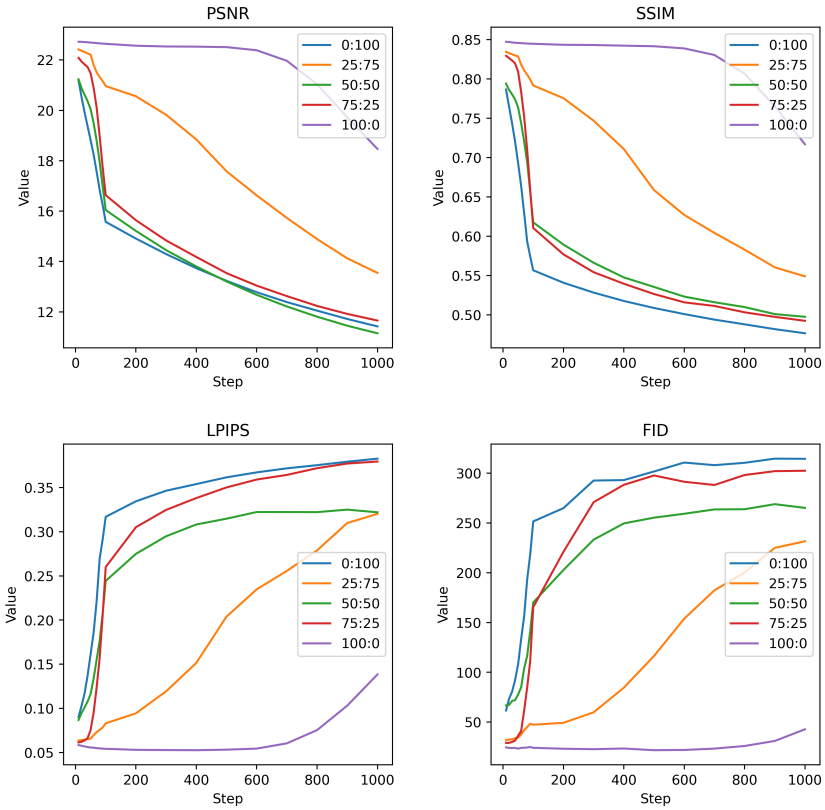


Figure 1: The descanning performance according to the reverse steps with respect to different ratios of synthetic data, i.e., $\{0\%, 25\%, 50\%, 75\%, 100\%\}$. For example, 75:25 denotes that the original data to synthetic data ratio is 75% and 25%, respectively, in the training set. The performance is measured in terms PSNR, SSIM, LPIPS, and FID of descanned images.

use of synthetic data for a high number of reverse steps.

Meanwhile, DescanDiffusion variants trained on DESCAN-18K with synthetic data achieve the best performance with only a few reverse steps. However, when a larger number of steps are employed, we found that there was a tendency to excessively remove degradations from scanned images, resulting in damaging the genuine appearance of original images. Therefore, a value of 10 is selected for T_o in that scenario. For DescanDiffusion trained on original DESCAN-18K, we select T_o as 200.

Testing performances of DescanDiffusion variants trained on a different ratio of synthetic data are shown in Table. 1. In the case of using synthetic data, it is best to train our model using original data and synthetic data at a ratio of 75:25. Therefore, we adopt that model as DescanDiffusion+ in the main paper.

Dataset Statistics

In this section, by providing reasonable statistics, we illustrate that our DESCAN-18K has more complex and local variant degradation than datasets used in other image restoration fields. We choose the popular datasets DIV2K (Timofte et al. 2018) and SIDD (Abdelhamed, Lin, and Brown 2018) utilized in super-resolution and denoising tasks which are well-known image restoration tasks, to compare with the DESCAN-18K dataset. For DIV2K, we perform the bicubic interpolation with an upscale factor of 4 to match the size of the low-resolution image with the high-resolution image.

SSIM (Wang et al. 2004) is an effective metric to measure the perceptual quality between two images by using three representative perceptual quality cues, i.e., luminance, contrast, and structure. In this paper, we explore statistics for degradations in datasets in terms of the aforementioned three factors. Our underlying assumption is that if the estimated visual quality between the target and degraded images in the dataset is relatively low, this dataset contains more complex degradations that are difficult to eliminate by a model.

We compare the average similarity of luminance, contrast, and structure for each image in different datasets. Let μ_x, μ_y, σ_x, σ_y, and σ_{xy} be the the average of x, the average of y, the variance of x, the variance of y, and the covariance of x and y, respectively. In this case, x and y are different images with the same dimension, respectively.

In (Wang et al. 2004), luminance(l), contrast(c) and structure(s) similarities are defined as

$$l(x, y) = \frac{2\mu_x\mu_y + c_1}{\mu_x^2 + \mu_y^2 + c_1}, \tag{1}$$

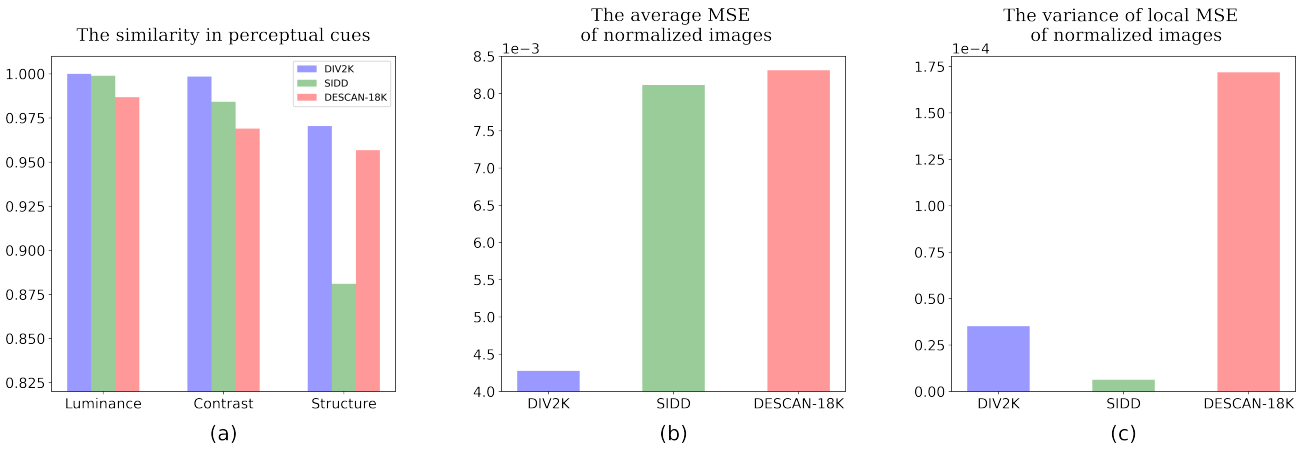
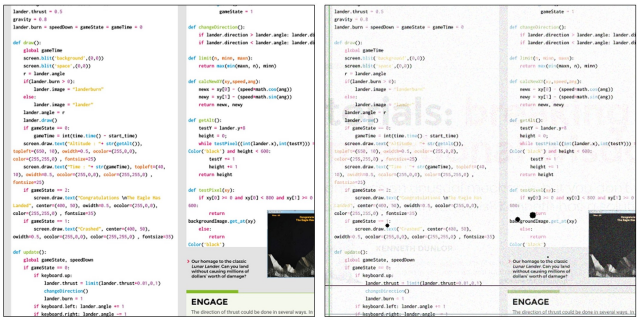


Figure 2: The statistics for DIV2K, SIDD, and DESCAN-18K: (a) The similarity in perceptual cues (luminance, contrast, and structure), (b) The average MSE of normalized images, (c) The variance of local MSE of normalized images.



Original Image Synthetic Image

Figure 3: An example of synthetic data. In Table. 2, we provide visual examples of each degradation discussed in the main paper by displaying them in individual patches.

$$c(x,y) = \frac{2\sigma_x\sigma_y + c_2}{\sigma_x^2 + \sigma_y^2 + c_2}, \tag{2}$$

$$s(x,y) = \frac{\sigma_{xy} + c_3}{\sigma_x\sigma_y + c_3}, \tag{3}$$

where $c_1 = (k_1 L)^2$, $c_2 = (k_2 L)^2$, $c_3 = c_2/2$ with $k_1 = 0.01$, $k_2 = 0.03$, and $L = 255$ (Wang et al. 2004).

Fig. 2 shows the statistics of the three datasets, i,e., DIV2K, SIDD, and DESCAN-18K in terms of: (a) the similarity in perceptual cues (luminance, contrast, and structure (Wang et al. 2004)); (b) the average MSE (Mean Squared Error) of normalized images; (c) the variance of local MSE of normalized images, aiming to measure the degree of diversity for local degradations.

In Fig. 2 (a), the luminance similarity of DIV2K and SIDD are both close to 1. However, DESCAN-18K has not only smaller luminance similarity but also contrast similarity than the two datasets, indicating that DESCAN-18K is comprised of images with a big gap between the target and degraded images in the perspective of background luminance/colors and contrast. This is because DESCAN-18K contains multiple complicated degradations that severely change background luminance/colors and contrast. On the other hand, as shown in Fig. 2 (a), the structural similarity is the lowest in SIDD, followed by DESCAN-18K. Note that, for structure, the higher the value, the higher the correlation between the two images is. Since SIDD has degradations akin to AWGN (additive white Gaussian noise) caused by various ranges of ISOs throughout the whole image region, the structure is broken in the degraded images, making the structure values smaller than DESCAN-18K.

However, the critical point is that DESCAN-18K has more diverse degradation than those noises. That is, although DESCAN-18K does not have much degradation that dramatically damages the image correlation (i.e., structure), DESCAN-18K is more complex than other datasets because several degradations are mixed and highly local variants.

To prove the aforementioned claims, we first measure the average of the MSE between each normalized image, i.e., the global variance of the residual. Next, we crop each residual to a patch of size 32×32 and calculate the MSE of each cropped patch. Finally, the variance for the local MSEs is measured to identify that the degradations in DESCAN-18K are local variants.

In Fig. 2 (b), DESCAN-18K shows the highest value in the average MSE of normalized images. That is, DESCAN-18K is degraded more complicated than other datasets at the global level. Moreover, in Fig. 2 (c), DESCAN-18K has the variance of local MSE by a significantly higher margin than the other two datasets. Therefore, it can be concluded that our dataset has a more diverse distribution of local degradations, which makes restoration problems more difficult, than in other datasets.

Detailed Settings for Synthesizing Degradations of Scanned Images

We detail the parameter settings for synthesizing degradations of scanned images in Table. 2. For each sample, degradation parameters are selected randomly with a uniform dis-

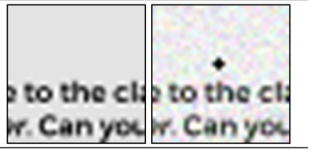
Degradation	Parameter	Range	Remarks	Patch Example
Bleed-through Effect	α probability	$[0.85, 0.95]$ 0.7	`cv2.addWeighted`	
Color Transition	factor probability	(i) $[1.2, 1.5]$ (ii) $[0.2, 0.4]$ (i) 0.3 (ii) 0.7	`cv2.cvtColor` `cv2.merge`	
Texture Distortion Halftone Pattern	type mean of Gaussian sigma of Gaussian probability	['*Gaussian*'] $[5, 10]$ $[10, 20]$ 1.0	-	
External Noise	center radius color thickness probability	$([0, H], [0, W])$ $[1, 5]$ $[200, 255]$ -1 0.3	`cv2.circle`	
Internal Noise	# of horizontal line # of vertical line (R, G, B) color value line starting position thickness probability	$[1, 5]$ $[1, 5]$ $([0, 255], [0, 255], [0, 255])$ $[0, H], [0, W]$ 1 0.5	`cv2.line`	

Table 2: Detailed parameter settings for synthesizing degradations of scanned images. Each scanned image has $H \times W$ resolution. Here, 'probability' in the 'Parameter' row for all degradation types indicates the probability of synthesizing that degradation. For the 'Color Transition' row, the 'factor' denotes the value multiplied by saturation in HSV space and the 'Range' column in the same row uses values from (i) and (ii) to indicate the cases at which saturation becomes strong and weak, respectively. That is, as the factor is greater than 1, the color becomes darker, and as the factor is less than 1, the color becomes lighter. The 'Remarks' row denotes the OpenCV (Bradski 2000) functions mainly utilized to implement each degradation. The 'Patch Example' row shows synthesized degradation examples extracted from the synthetic image in Fig. 3.

tribution. Synthetic data are generated using original images from a subset of the DESCAN-18K training set.

Note that although there are Pillow (Umesh 2012) functions that can implement the halftone pattern, we found that it is difficult to generate specific halftone patterns in the scanned image of DESCAN-18K with this method. Meanwhile, texture distortions and halftone patterns can result in a scanned image that appears noisy. Therefore, we aim to incorporate these two degradations by using isotropic Gaussian noise. Fig. 3 shows an example of synthesized data.

	Text region (%)	Image region (%)	# of pairs
Train	23.47	76.53	17,640
Val	23.47	76.53	360
Test	31.58	68.42	360
Train + Val + Test	23.63	76.37	18,360

Table 3: The distribution of image and text regions in DESCAN-18K.

Analysis on Distribution of Image and Text Regions in DESCAN-18K

Most documentation restoration (Verma and Malik 2015; Bhasharan, Konstantinides, and Beretta 1997) and real-world photo restoration tasks (Wan et al. 2020; Ho and Zhou 2022; Yu et al. 2022; Chen et al. 2021) handle either text or image contents. On the other hand, our DESCAN-18K has compound content with a variety of images and texts.

To further analyze DESCAN-18K, we compute the ratio of the image and text regions in each data using the text detection pre-trained model from the docTR (Mindee 2021) library. Specifically, we employ the DBNet (Liao et al. 2020), using a ResNet-50 (He et al. 2016) backbone for text detection. In Table. 3, DESCAN-18K approximately has 1:3 ratios in text and image regions as made with magazines.

Examples of Degradations in the Scanned Image

This section introduces more diverse degradation examples. See Fig. 4, 5, and 6. In some cases, two or more of each degradation appear together rather than alone. Note that we

zoom in for other degradations but not color transition because it usually occurs globally.

More Qualitative Comparisons

To visualize the effectiveness of our DescanDiffusion, we add a significant volume of qualitative results comparing our model to other methods and commercial products. Fig. 7, 8, 9, and 10 shows the comparison with various approaches. Our DescanDiffusion outperforms comparable methods and commercial products by a substantial margin in visual quality. Especially, our model is more effective in removing internal noise in liner laser patterns than other approaches, and DescanDiffusion+ with the synthetic data generation scheme produces more outstanding results in this case.

Discussion and Limitation

Although our DescanDiffusion has achieved remarkable performance over other approaches, it has limitations in some cases. Fig. 11 shows the failure cases of our method.

Fig. 11 (a) and (b) show examples that our model mistakenly recognizes the intentional noise and texture in the original image as degradation and excessively removes it, resulting in an unnaturally smooth texture.

In our future works, we plan to enhance the generalization of the dataset by collecting additional real scanned-original image pairs or synthesizing data using a deliberate hyperparameter tuning strategy. Additionally, we will aim to explore model architectures that are better suited for handling multiple degradations.

References

Abdelhamed, A.; Lin, S.; and Brown, M. S. 2018. A High-Quality Denoising Dataset for Smartphone Cameras. In *IEEE Conference on Computer Vision and Pattern Recognition (CVPR)*.

Bhasharan, V.; Konstantinides, K.; and Beretta, G. 1997. Text and image sharpening of scanned images in the JPEG domain. In *Proceedings of international conference on image processing*, volume 2, 326–329. IEEE.

Bradski, G. 2000. The OpenCV Library. *Dr. Dobb's Journal of Software Tools*.

Chen, X.; Liu, Y.; Zhang, Z.; Qiao, Y.; and Dong, C. 2021. HDRUnet: Single image HDR reconstruction with denoising and dequantization. In *Proceedings of the IEEE/CVF Conference on Computer Vision and Pattern Recognition*, 354–363.

Elfwing, S.; Uchibe, E.; and Doya, K. 2018. Sigmoid-weighted linear units for neural network function approximation in reinforcement learning. *Neural Networks*, 107: 3–11.

He, K.; Zhang, X.; Ren, S.; and Sun, J. 2016. Deep residual learning for image recognition. In *Proceedings of the IEEE conference on computer vision and pattern recognition*, 770–778.

Heusel, M.; Ramsauer, H.; Unterthiner, T.; Nessler, B.; and Hochreiter, S. 2017. Gans trained by a two time-scale update rule converge to a local nash equilibrium. *Advances in neural information processing systems*, 30.

Ho, M. M.; and Zhou, J. 2022. Deep Photo Scan: Semi-Supervised Learning for dealing with the real-world degradation in Smartphone Photo Scanning. In *Proceedings of the IEEE/CVF Winter Conference on Applications of Computer Vision*, 1880–1889.

Kingma, D. P.; and Ba, J. 2014. Adam: A method for stochastic optimization. *arXiv preprint arXiv:1412.6980*.

Liao, M.; Wan, Z.; Yao, C.; Chen, K.; and Bai, X. 2020. Real-time scene text detection with differentiable binarization. In *Proceedings of the AAAI conference on artificial intelligence*, volume 34, 11474–11481.

Mindee. 2021. docTR: Document Text Recognition. https://github.com/mindee/doctr.

Nichol, A. Q.; and Dhariwal, P. 2021. Improved denoising diffusion probabilistic models. In *International Conference on Machine Learning*, 8162–8171. PMLR.

Ronneberger, O.; Fischer, P.; and Brox, T. 2015. U-net: Convolutional networks for biomedical image segmentation. In *International Conference on Medical image computing and computer-assisted intervention*, 234–241. Springer.

Timofte, R.; Gu, S.; Wu, J.; and Van Gool, L. 2018. Ntire 2018 challenge on single image super-resolution: Methods and results. In *Proceedings of the IEEE conference on computer vision and pattern recognition workshops*, 852–863.

Umesh, P. 2012. Image Processing in Python. *CSI Communications*, 23.

Vaswani, A.; Shazeer, N.; Parmar, N.; Uszkoreit, J.; Jones, L.; Gomez, A. N.; Kaiser, Ł.; and Polosukhin, I. 2017. Attention is all you need. *Advances in neural information processing systems*, 30.

Verma, R. N.; and Malik, L. G. 2015. Review of illumination and skew correction techniques for scanned documents. *Procedia Computer Science*, 45: 322–327.

Wan, Z.; Zhang, B.; Chen, D.; Zhang, P.; Chen, D.; Liao, J.; and Wen, F. 2020. Bringing old photos back to life. In *proceedings of the IEEE/CVF conference on computer vision and pattern recognition*, 2747–2757.

Wang, Z.; Bovik, A.; Sheikh, H.; and Simoncelli, E. 2004. Image quality assessment: from error visibility to structural similarity. *IEEE Transactions on Image Processing*, 13(4): 600–612.

Yu, X.; Dai, P.; Li, W.; Ma, L.; Shen, J.; Li, J.; and Qi, X. 2022. Towards Efficient and Scale-Robust Ultra-High-Definition Image Demoiréing. In *European Conference on Computer Vision*, 646–662. Springer.

Zhang, R.; Isola, P.; Efros, A. A.; Shechtman, E.; and Wang, O. 2018. The unreasonable effectiveness of deep features as a perceptual metric. In *Proceedings of the IEEE conference on computer vision and pattern recognition*, 586–595.

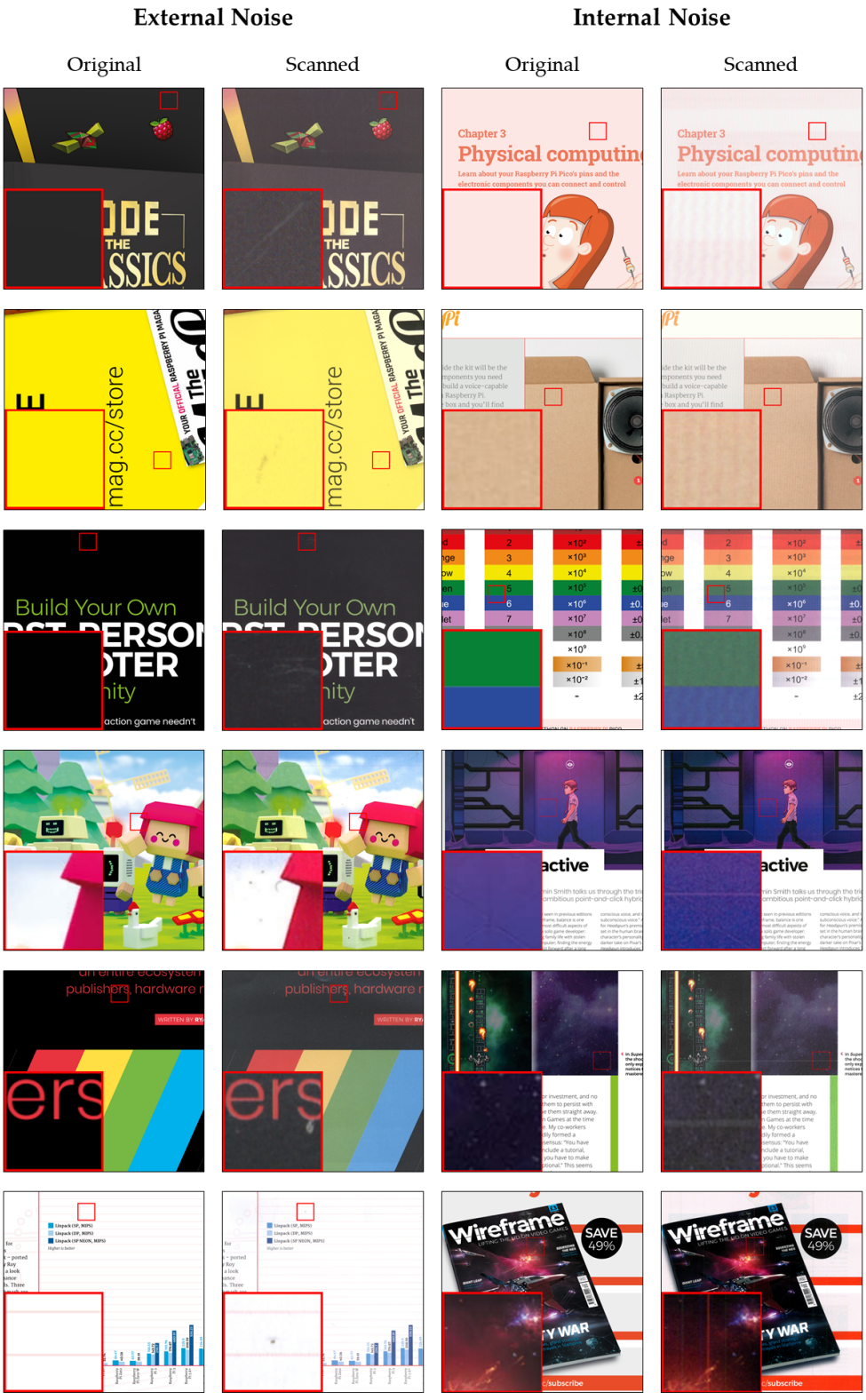


Figure 4: Examples of degradations in the scanned image: external noise and internal noise. For external noise, the above three columns are examples of localized stains, and the lower three columns represent examples of dot degradations. For internal noise, the above three columns are examples of curved laser patterns, and the lower three columns are examples of linear laser patterns.

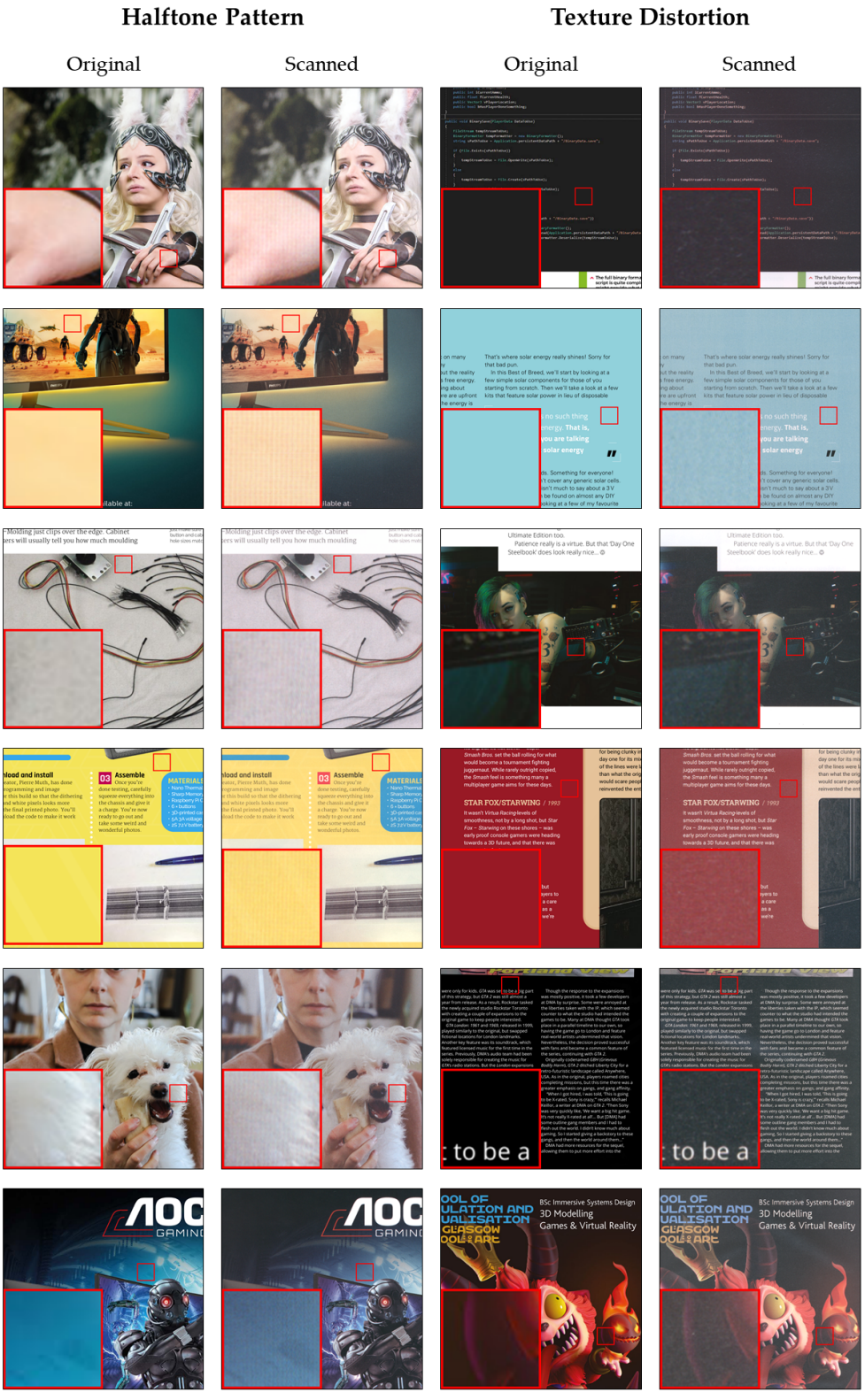


Figure 5: Examples of degradations in the scanned image: halftone pattern and texture distortion.

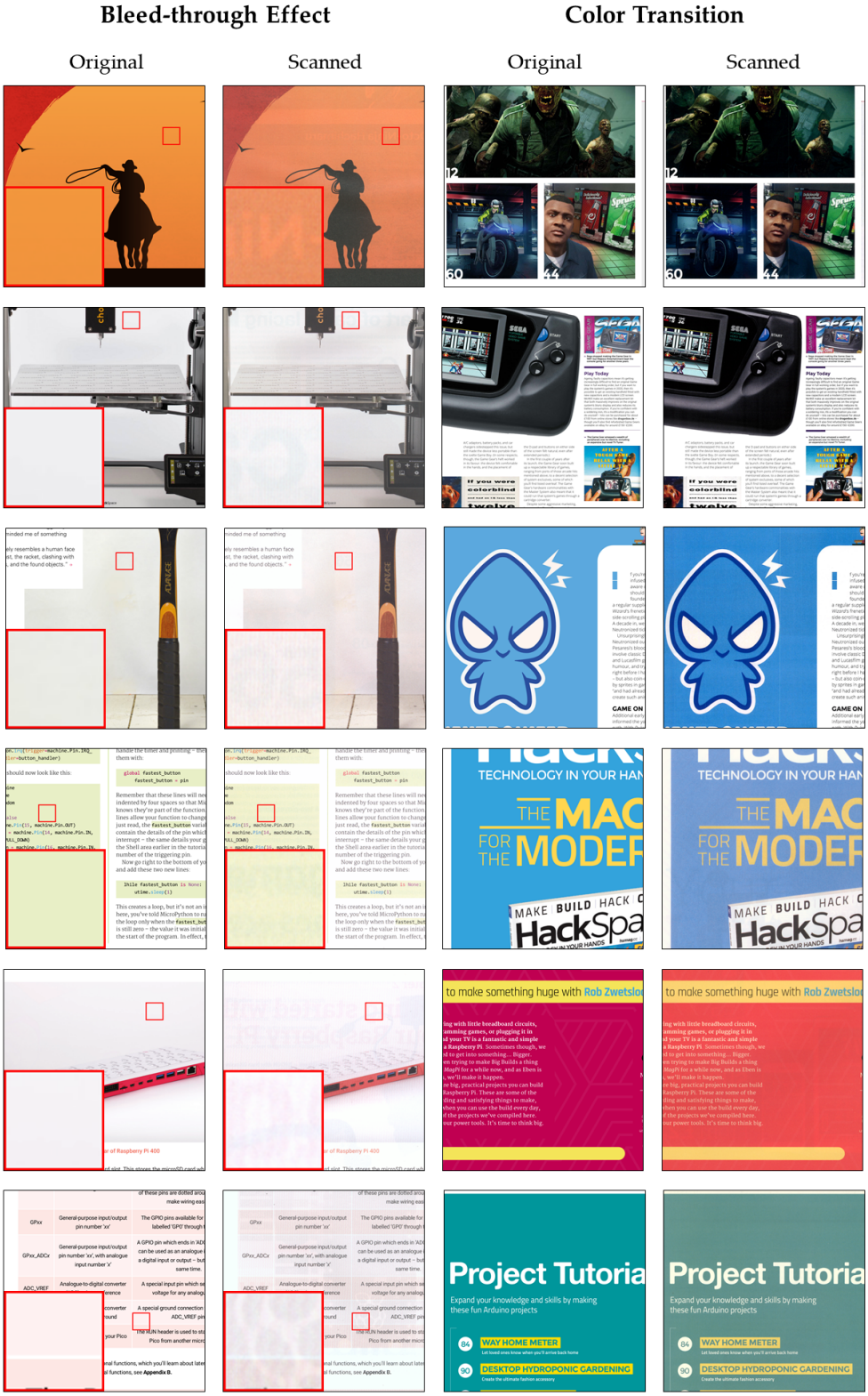


Figure 6: Examples of degradations in the scanned image: bleed-through effect and color transition. For color transition, the upper three columns are examples of color saturation, and the lower three columns are examples of color fading.

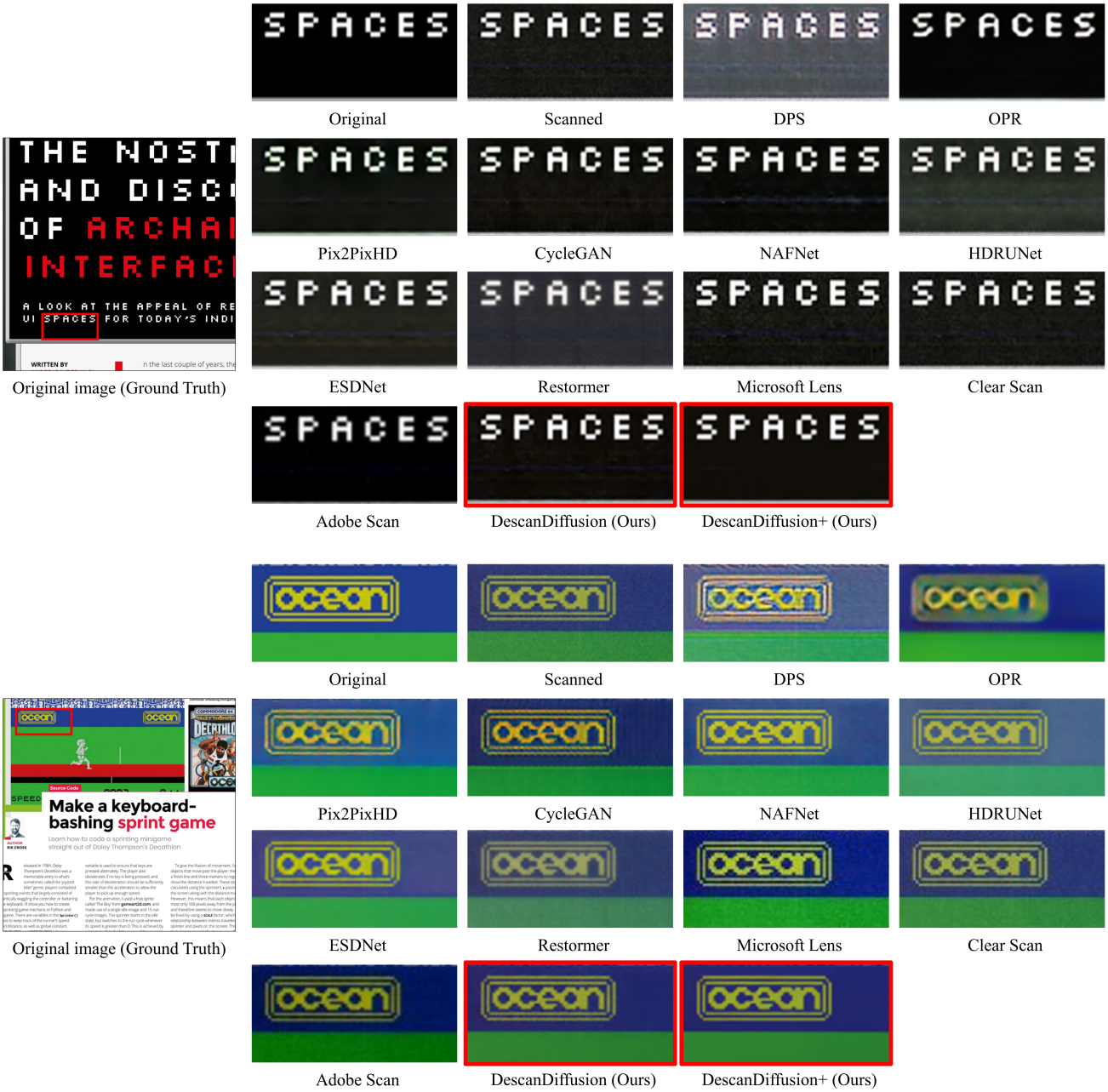


Figure 7: Additional qualitative comparisons of descanning performance on DESCAN-18K testing set (1). Zoom in for the best views.

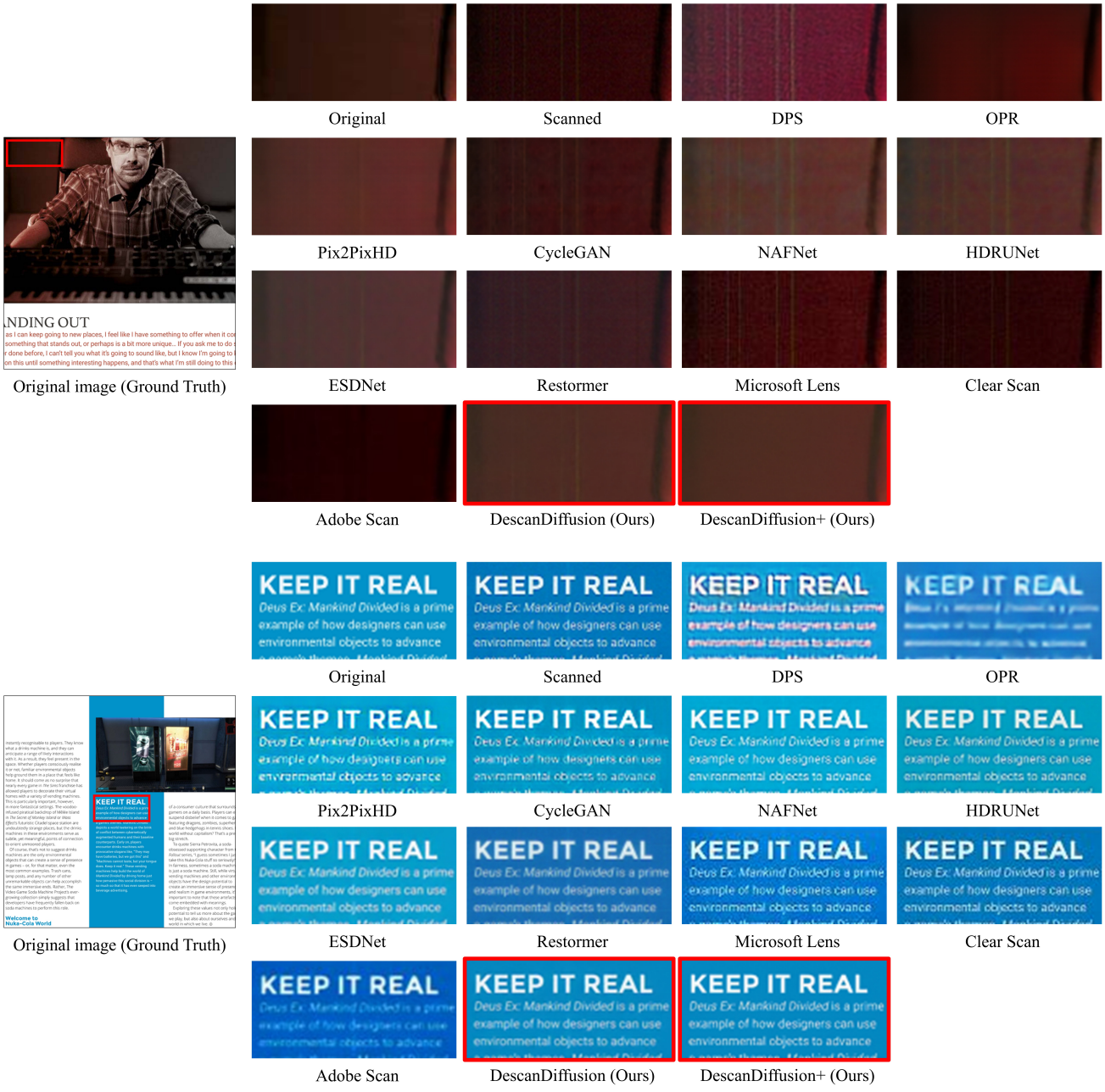


Figure 8: Additional qualitative comparisons of descanning performance on DESCAN-18K testing set (2). Zoom in for the best views.

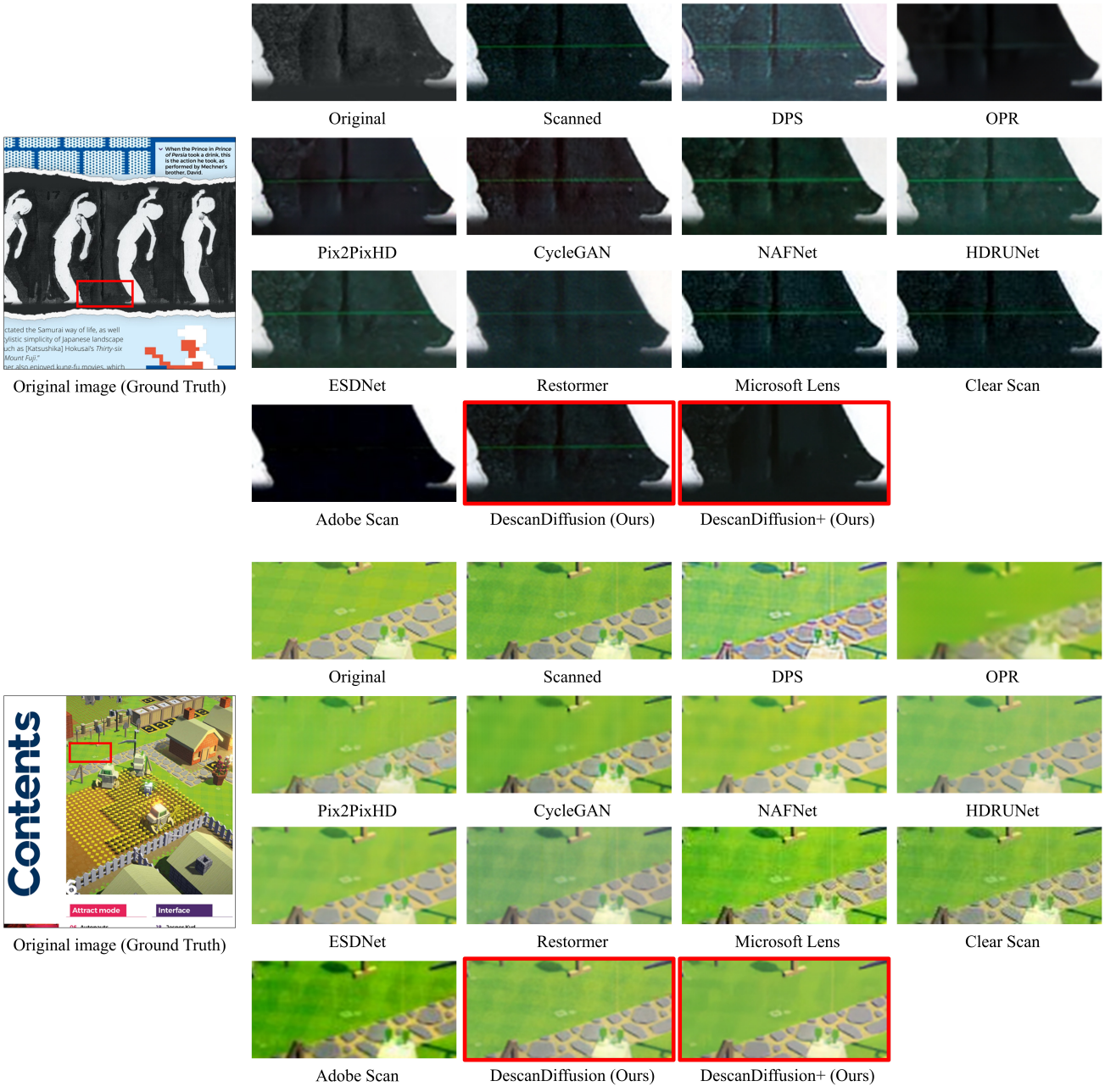


Figure 9: Additional qualitative comparisons of descanning performance on DESCAN-18K testing set (3). Zoom in for the best views.

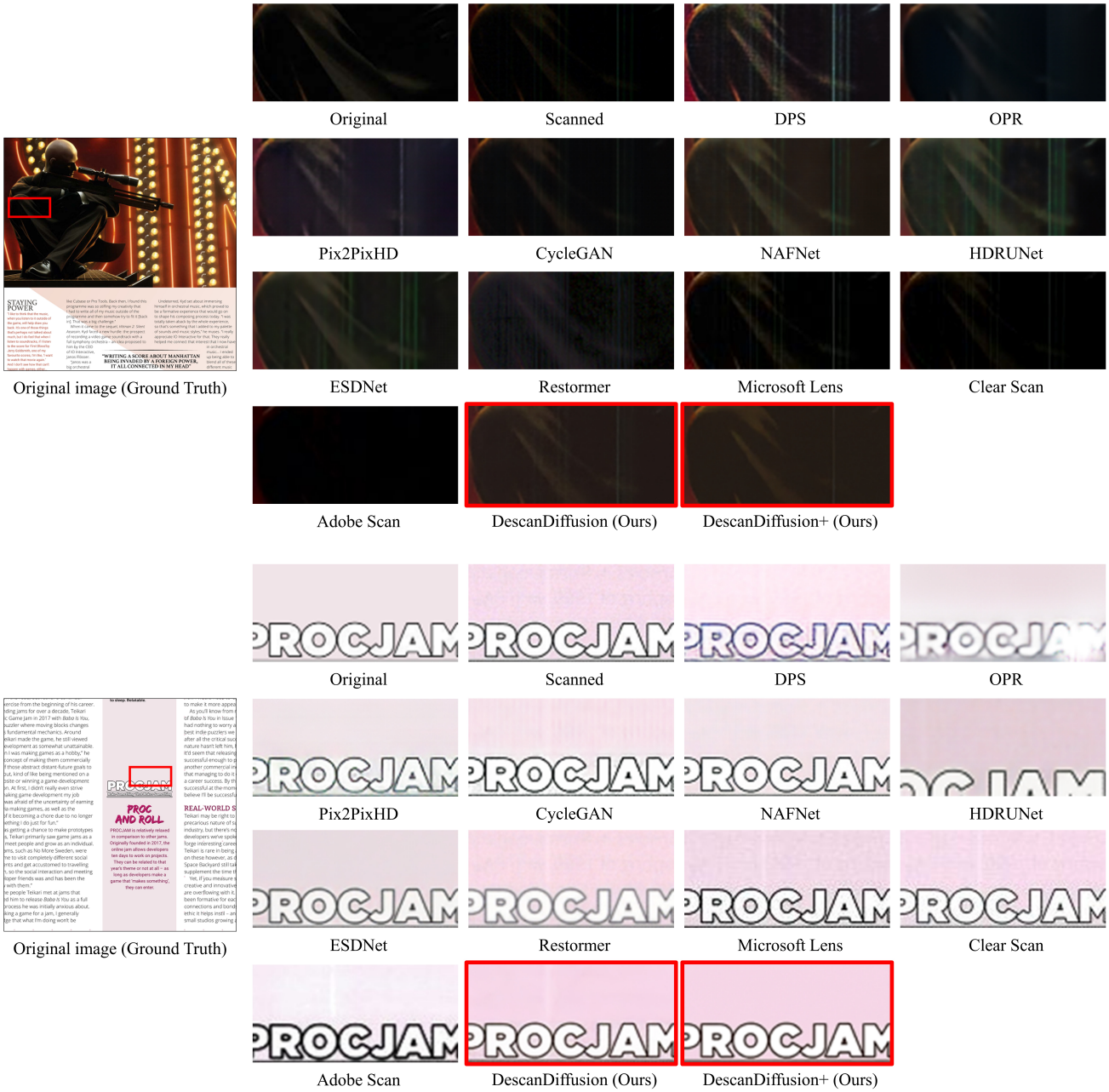


Figure 10: Additional qualitative comparisons of descanning performance on DESCAN-18K testing set (4). Zoom in for the best views.

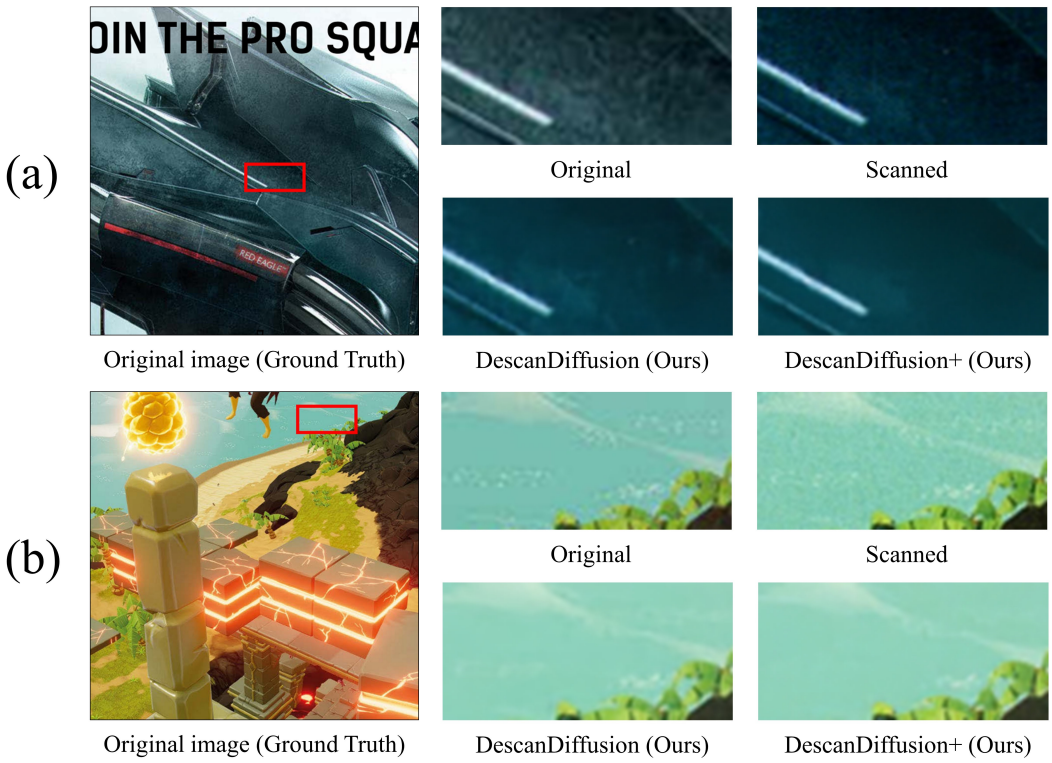


Figure 11: Failure cases of DescanDiffusion